ACS OMEGA

http://pubs.acs.org/journal/acsodf

Article

Effects of Silicon Dioxide/Graphene Oxide Hybrid Modification on Curing Kinetics of Epoxy Resin

Bingwang Gou, Xiuduo Song,* Zongkai Wu, and Xuebing Chen

Cite This: *ACS Omega* 2022, 7, 36551−36560

Read Online

ACCESS | Metrics & More | Article Recommendations

ABSTRACT: In this study, SiO_2-grafted graphene oxide (GO-SiO_2) was prepared using the oxygen-containing group on the GO surface as the active site of the reaction. The chemical structure, morphology, and particle size of GO and GO-SiO_2 were carefully investigated by Fourier transform infrared (FT-IR) spectroscopy, X-ray photoelectron spectroscopy (XPS), X-ray diffraction (XRD), Raman spectroscopy, thermogravimetry, transmission electron microscopy, scanning electron microscopy, and atomic force microscopy, and the results proved that the grafting modification was successful. Furthermore, epoxy (EP)/GO composites were prepared, and the effects of unmodified GO and GO-SiO_2 on the curing kinetics of EP were comparatively studied by differential scanning calorimetry (DSC). The results showed that, compared with neat EP and EP/GO, GO-SiO_2 significantly reduces the curing temperature of the composites, indicating that GO-SiO_2 has a more significant catalytic effect on the curing process of EP. The calculation results of the Kissinger method showed that the curing activation energy of EP/GO-SiO_2 is obviously lower than that of EP/GO and neat EP. Results of the Ozawa method showed that the introduction of GO-SiO_2 reduces the curing activation energy during the whole curing process, and in the middle and late stages of curing (α = 0.5−1) can significantly reduce the curing activation energy. The related mechanism has been proposed.

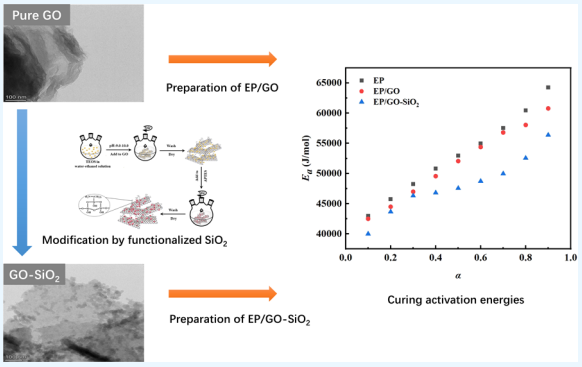

1. INTRODUCTION

Epoxy resin (EP) has excellent physical, mechanical, electrical insulation properties, bonding properties with various materials, and flexibility of use.[1−3] Therefore, it can be made into coatings, composites, adhesives, molding materials, and injection molding materials, and has been widely used in various fields of national economy.[4,5]

To endow epoxy resin with more excellent properties, nanofiller-modified EP has been widely studied in recent years.[6] Graphene oxide (GO) has a large specific surface area, excellent mechanical properties, optical and electromagnetic properties, and a large number of oxygen-containing groups on the surface and edges of the layer, such as −COOH, −OH, C−O−C, etc.[7,8] GO not only has certain electrical insulation properties but also provides reactive sites for chemical grafting modification, which seems to be an ideal filler for EP.[9−11] However, due to the stacking structure of GO, it is easy to agglomerate in the matrix, which greatly reduces its effective specific surface area, so it cannot give full play to the enhancement effect for the polymer matrix.[10] Therefore, further modification of GO is strongly needed to ensure its fine dispersion in the polymer matrix.[5,12]

SiO_2 is widely used in electronic and electrical fields as a filler because of its high dielectric strength, high resistivity, and chemical stability.[3,13] When it penetrates into the material, it will interact with the unsaturated bond of the polymer chain, improve the heat resistance, light and chemical stability of the material, and make the product antiaging and chemical corrosion resistant.[14,15] The modification of GO by SiO_2 can effectively solve the problem of easy agglomeration of GO,[16] which is conducive to increasing the number of active sites on the surface of GO,[16,17] so as to improve the comprehensive properties of the composites.[16−18]

The SiO_2-modified GO can be prepared by covalent and noncovalent bonds. Electrostatic interaction or chemical grafting is commonly used to introduce SiO_2 onto the GO surface. Great efforts have been made in this area, and many elegant works can be seen. Zhang et al.[19] prepared hybridized GO-SiO_2 nanoparticles by the method of physical blending, and reported that the hybridization of GO-SiO_2 was the determining factor for the reinforcement of the mechanical properties and elasticity of the NBR; Dong et al.[20] synthesized

Received: July 17, 2022
Accepted: September 23, 2022
Published: October 4, 2022

https://doi.org/10.1021/acsomega.2c04505
ACS Omega 2022, 7, 36551−36560

Scheme 1. Schematic Illustration of the Preparation of the SiO_2-Modified GO

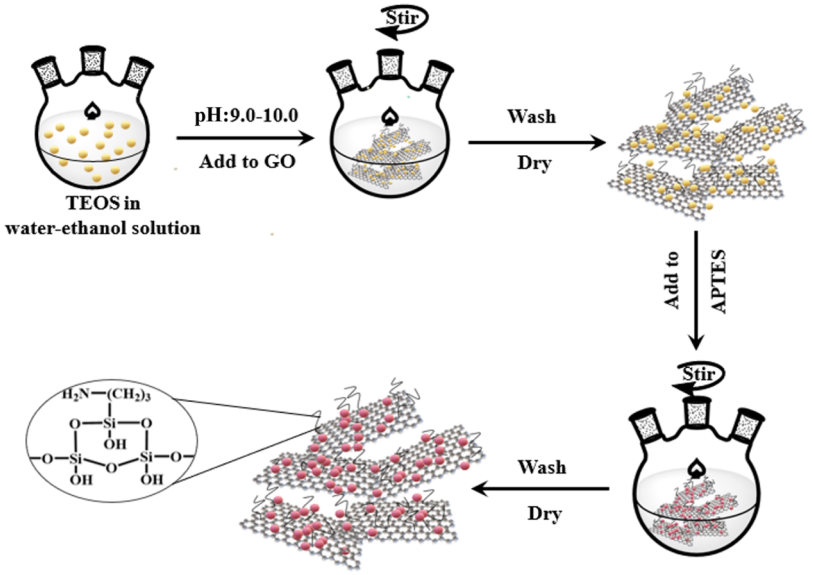

SiO_2-GO via in situ hydrolysis and condensation of tetraethylorthosilicate (TEOS) on the GO surface, and then they incorporated SiO_2-GO into styrene-butadiene rubber (SBR) latex to prepare an elastomer composite (SBR/SiO_2-GO); Dong et al.[14] reported a novel SiO_2−GO/acrylic resin nanocomposite. They prepared the nanohybrids of GO-SiO_2 by surface modification of GO by the hydrolysis of TEOS; Haddadi et al.[21] used the modified Hummer technique for the preparation of GO nanosheets, and then GO-SiO_2 nanosheets were synthesized via the sol−gel method. In their study, GO was functionalized with a silane mixture of TEOS and APTES (75:25, w/w) as the silicon precursor and surface modifier using the in situ hydrolysis process; Luo et al.[22] prepared GO-SiO_2 with different sizes via in situ preparation. Different sizes and weight fractions of GO/SiO_2 were added to the phenolic resin to prepare phenolic foam composites.

With respect to the modification of EP, current reports mainly focus on the enhancement of mechanical performance and corrosion properties. Damian et al.[3] reported a novel strategy, which uses the modified carbodiimide coupling mechanism between GO and SiO_2, they also compared it with a functionalization method, which creates physical interactions through ultrasonication. The synergistic effect of GO functionalized with SiO_2 nanostructures in the EP nanocomposites was then investigated; Zhang et al.[1] reported a facile method to SiO_2−GO. The effect of SiO_2−GO nanosheets on corrosion protection and barrier performance of the EP coating was investigated. Bouibed et al.[23] used tetraethylorthosilicate (TEOS) as a silica source to decorate the surface of graphene oxide (GO) nanosheets and the use of *N*-(*β*-aminoethyl)-*γ*-aminopropyl-trimethoxysilane (Z-6020) as a coupling agent through a one-step in situ sol−gel process to prepare GO-SiO_2. The effect of incorporating 0.1 wt % GO sheets and GO-SiO_2 nanohybrids on the corrosion protection and barrier performance of the epoxy coating was reported, they found that the incorporation of GO-SiO_2 into the epoxy matrix improved its thermal stability and corrosion protection performance. Wang et al.[13] reported a facile and rapid come close to the manufacture of advanced EP nanocomposites by grafting nano-SiO_2 onto GO through the thiol-ene click reaction. Nano-SiO_2 has been successfully grafted onto GO via covalent bonding, which effectively improved interface compatibility and dispersion in the EP matrix. The reinforcing mechanisms of the mechanical performance had also been elaborated; Ramezanzadeh et al.[11] reported two facile routes for the synthesis and characterization of SiO_2-GO by a two-step in situ sol−gel process using a mixture of 3-aminopropyl triethoxysilane and tetraethylorthosilicate in water−alcohol solution. The effect of SiO_2-GO nanohybrids on corrosion protection and barrier performance of the EP coating was investigated.

As summarized above, current studies mainly focus on the mechanical and corrosion performance of EP, however, the curing kinetics, which plays an important role in determining the final performances of the composites, has not been reported. In this paper, a chemical grafting method was used to prepare SiO_2-modified GO (GO-SiO_2). EP/GO nanocomposites were prepared, and the curing kinetics of EP/GO nanocomposites were comparatively investigated to study the impact of GO-SiO_2 on the curing kinetics of the composites.

2. EXPERIMENTAL SECTION

2.1. Materials. Bisphenol A epoxy resin (industrially pure, grade E51, epoxy equivalent 184−195 g/mol) was purchased from China Deyuan Chemical Co., Ltd., China; GO with an average particle size of 191.10 nm was purchased from Deyang Alkene Carbon Technology Co., Ltd., China; amine curing agent JH-0422 (amine value 750−850 mg KOH/g) was purchased from Changshu Jiafa Chemical Co., Ltd., China; hydrophilic vapor phase nanosilica (SiO_2, hydraulic-150 type, specific surface area 150 m^2/g, particle size 7−40 nm, 99.8%) was purchased from Shanghai Aladdin Biochemical Technology Co., Ltd., China; *γ*-aminopropyl triethoxysilane (silane coupling agent KH550, APTES, 98%) was purchased from Chengdu Zhuopu Instrument Co., Ltd., China. Ammonia ($NH_3{\cdot}H_2O$), tetraethoxysilane (TEOS, SiO_2 content ≥28.4%, density 0.932−0.936 g/mL), xylene, and ethanol (CH_3CH_2OH) were of analytical purity.

2.2. Sample Preparation. *2.2.1. Preparation of SiO_2-Modified GO.* GO-SiO_2 was prepared by chemical grafting. In this process, 0.2 g of GO, 600 mL of ethanol, and 150 mL of

https://doi.org/10.1021/acsomega.2c04505
ACS Omega 2022, 7, 36551−36560

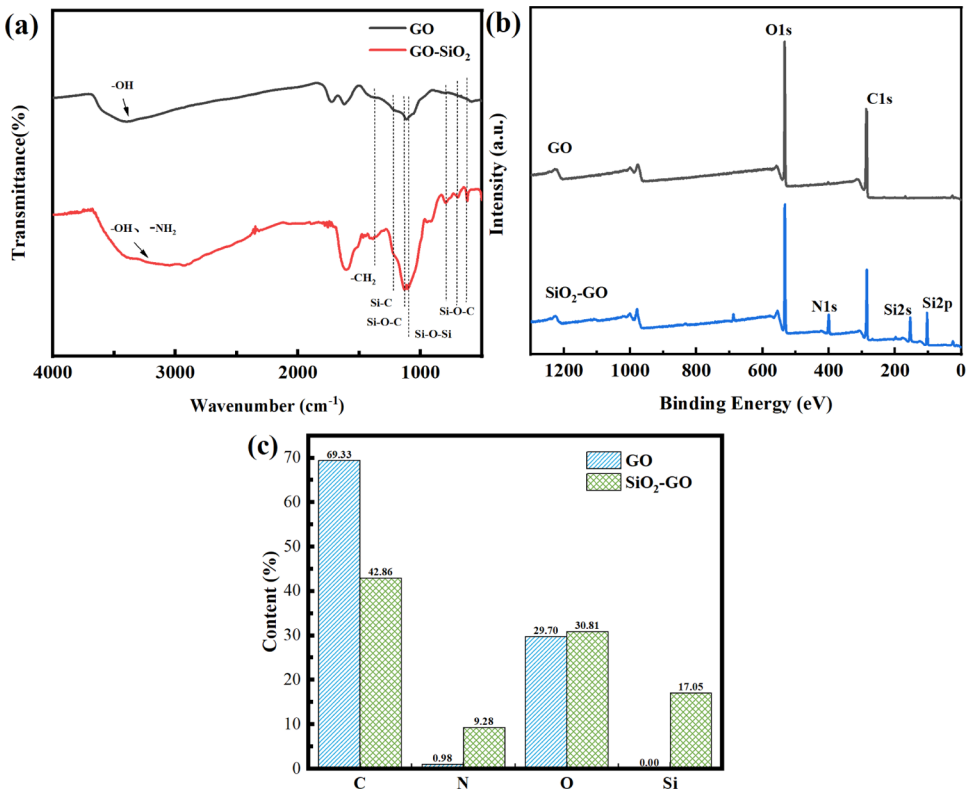

Figure 1. (a) FT-IR spectra, (b) XPS survey spectrum, and (c) elemental contents of the samples of GO and GO-SiO_2.

H_2O were added to the beaker, and ultrasonically treated at room temperature for 1 h. Then, ammonia solution was dropped to adjust the pH of the solution to 9.0−10.0, and then 10 mL of TEOS was added. After ultrasonic treatment at room temperature for 12 h, the obtained mixed solution was centrifuged at a rate of 5000 r/min, and then washed with ethanol 3 times. After that, 5 mg of APTES, 600 mL of ethanol, and 150 mL of H_2O, respectively, were added to a flask and then placed in an oil bath at 50 °C. It should be emphasized that the addition of APTES is of great importance, which provides strong interaction between GO and SiO_2. After that, they were treated with magnetic stirring for 5 h. Finally, the mixed solution was repeatedly washed with ethanol 3 times, and then it was placed in a vacuum oven at 90 °C for 24 h after suction filtration, and then dried to remove the remaining ethanol. The resulting product is named GO-SiO_2. The preparation process is shown in Scheme 1.

2.2.2. Preparation of EP/GO Composites. To prepare EP/GO composites, 0.02 g of GO (untreated GO or GO-SiO_2) and 400 mL of ethanol were added to the beaker and sonicated at room temperature for 2 h. Then, 4 g of EP was added and sonicated at room temperature for 2 h. After that, they were stirred (250 rpm) at 90 °C for 12 h to evaporate the ethanol, and then placed in a vacuum oven at 90 °C for 2 h to remove the remaining ethanol. Finally, the JH-0422 amine curing agent with a mass fraction of 20% was added to the system and stirred until the system was uniformly mixed. The obtained samples were named EP/GO and EP/ GO-SiO_2, respectively.

2.3. Characterizations. *2.3.1. Fourier Transform Infrared Spectroscopy (FT-IR).* The FT-IR spectra of the samples were recorded in transmission mode using a Fourier transform infrared spectrometer (PerkinElmer Frontier, PerkinElmer Corp.). The scanning range was 4000−400 cm^{-1}, the accuracy is 4 cm^{-1}, and the scanning times were 16.[24−27]

2.3.2. X-ray Photoelectron Spectroscopy Analysis (XPS). The surface chemical structure and composition of GO samples were analyzed by X-ray photoelectron spectroscopy (Thermo Scientific k-α, Thermofisher Corp.). The test condition is vacuum degree 5 × 10^{-9} mbar, monochrome alka source (mono alka), with an energy of 1486.6 eV, voltage of 15 kV, beam current of 15 mA, CAE analyzer scanning mode, and instrument working function of 4.2.[8,27]

2.3.3. X-ray Diffraction (XRD). The X-ray diffraction (XRD) pattern of GO was tested using an X-ray diffractometer (Ultima IV, RIGAKU Corp., Japan). Cu K-α Radiation wavelength λ = 0.154 nm, scanning speed 10 °/min powder samples were used and 2θ = 0−90° was recorded.

2.3.4. Raman Spectra. The structure of GO was analyzed using a Raman spectrometer (Renishaw Invia, Bruker Corp., U.K.). The wavelength of the laser was 514 nm.

2.3.5. Thermogravimetric Analysis (TGA). The thermal stability of GO was analyzed by thermogravimetric analysis (TGA, FG 209 F1, Netzsch Corp., Germany). About 2 mg of GO powder was weighed and placed in a crucible at a heating rate of 10 °C/min under a N_2 atmosphere. The temperature range was 30−800 °C.[10,26,28]

2.3.6. Transmission Electron Microscopy (TEM). To further analyse the structure of GO, transmission electron microscopy (TEM, TECNAI G2 F20 s-twin, FEI Corp.) was carried out at an accelerating voltage of 200 kV. TEM samples were dispersed in ethanol and deposited on the copper grid for observation.

2.3.7. Scanning Electron Microscopy Analysis (SEM). A scanning electron microscope (Zeiss Gemini 300, Carl Zeiss AG, Germany) was used to observe morphologies of GO and

https://doi.org/10.1021/acsomega.2c04505
ACS Omega 2022, 7, 36551−36560

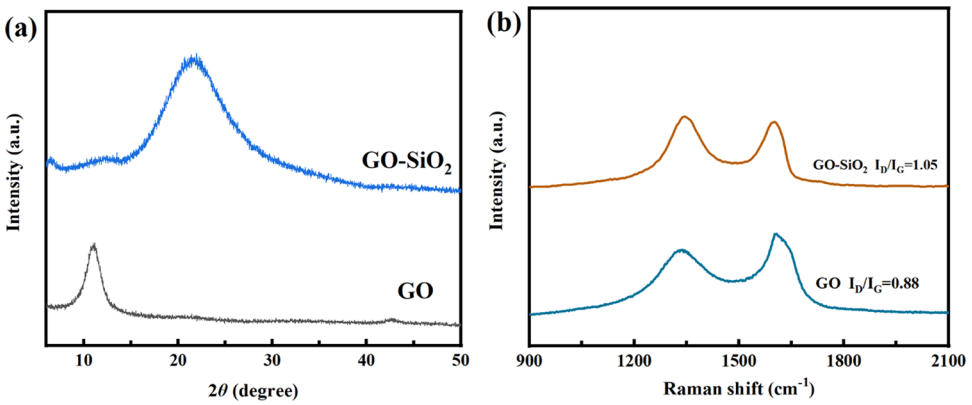

Figure 2. (a) XRD patterns and (b) Raman spectra of GO and GO-SiO_2.

modified GO. Before measurement, the impact fracture surface of the sample was coated with gold.[25,27,29,30]

2.3.8. Atomic Force Microscopy (AFM). An atomic force microscope (AFM) (Asylum Research MFP-3D, Oxford Instruments, U.K.) under the tapping mode was used to study the morphology of the fillers.[30,31]

2.3.9. Differential Scanning Calorimetry (DSC). All non-isothermal curing kinetics experiments were carried out with a differential scanning calorimeter (DSC3+, Mettler Toledo Corp., Switzerland) under a nitrogen flow of 50 mL/min. The standard procedure for each test is as follows: 5−8 mg of the sample was heated to 300 °C at different heating rates of 5, 10, 15, and 20 °C/min, respectively, and the heating curves were recorded.[32]

3. RESULTS AND DISCUSSION

3.1. Characterization of the Modified GO. The chemical structure and elemental composition of GO and GO-SiO_2 were studied by FT-IR and XPS, the obtained results are shown in Figure 1. Figure 1a shows the FT-IR spectra of GO and GO-SiO_2. For both GO and GO-SiO_2, the wide peak in the infrared spectrum at about 3400 cm^{-1} can be seen, which corresponds to the −OH stretching vibration. For, GO-SiO_2, some new peaks can be seen: the stretching vibration peak of Si−C appears at about 1230 cm^{-1}, the asymmetric stretching vibration peaks of the −Si−O−C−/−Si−O−Si− bond appear at about 1130 and 1090 cm^{-1}, the symmetric stretching vibration absorption peak of the −Si−O−Si− bond appears at about 800 cm^{-1}, the vibration peak of −Si−O−C− appears at about 630 cm^{-1}, and the wide peak appears at about 3000 cm^{-1} corresponding to the amine group. These results indicate that SiO_2 has been successfully chemically grafted to the GO surface.

Figure 1b,c shows the XPS results of GO and GO-SiO_2. It can be seen that O_{1s}, C_{1s}, and N_{1s} are the main element signal peaks of GO. In addition to the above element signal peaks, Si 2s and Si 2p signal peaks also appear in GO-SiO_2, indicating that SiO_2 has been successfully introduced into the GO surface. Further calculation shows that the C/O ratio of GO-SiO_2 is 1.39, which is lower than the C/O ratio of GO of 2.33; the O/Si ratio of GO-SiO_2 is 1.81, indicating that it has a large amount of silane chemical grafting.

Figure 2a shows the XRD profiles of GO and GO-SiO_2. For GO, a strong peak at 2θ = 12° can be seen, which becomes very weak for GO-SiO_2. Instead, a strong and wide peak at 2θ = 21° can be observed in the XRD profile of GO-SiO_2, which is caused by the diffraction of amorphous silicon produced by SiO_2. Figure 2b shows the Raman spectra of GO and GO-SiO_2. The *D* peak (1360 cm^{-1}) of GO is formed by the sp^3 hybrid part, which represents the atomic lattice defects caused by C−C disordered vibration. The *G* peak (1600 cm^{-1}) is produced by the in-plane vibration of sp^2 carbon atoms. The ratio of I_D/I_G can reflect the degree of surface defects of GO. Through calculation, the I_D/I_G of GO-SiO_2 is found to be greater than that of GO, and the *G* peak shifts to the right, indicating that its surface has more defects. This may be because SiO_2 has been successfully introduced into the GO surface, causing certain damage to its structure, and the modified GO layers were divided successfully. The I_D/I_G value of GO-SiO_2 is 1.05, which is significantly higher than 0.88 of unmodified GO, indicating that the chemical structure of the surface of GO-SiO_2 has changed, that is, after the hydrolysis of TEOS, there is a chemical interaction with GO, and the chemical grafting is successful.

Figure 3 shows the thermogravimetric curves of GO and GO-SiO_2. The thermal stability of GO is relatively poor, and

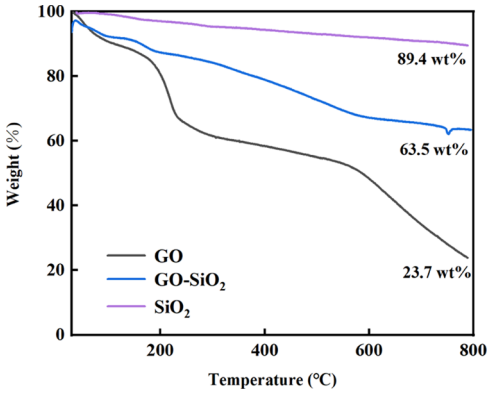

Figure 3. TGA curves of GO and GO-SiO_2.

the thermal residual weight at 800 °C is 23.7%. Its thermal weight loss can be roughly divided into three stages. In the first stage, the weight loss temperature is lower than 100 °C, which is caused by the evaporation of free water and combined water. In the second stage, the weight loss temperature is about 200 °C, which is mainly caused by the decomposition and vaporization of oxygen-containing functional groups of GO. The third stage begins to lose weight at 500 °C, mainly due to the decomposition of the carbon skeleton.

https://doi.org/10.1021/acsomega.2c04505
ACS Omega 2022, 7, 36551−36560

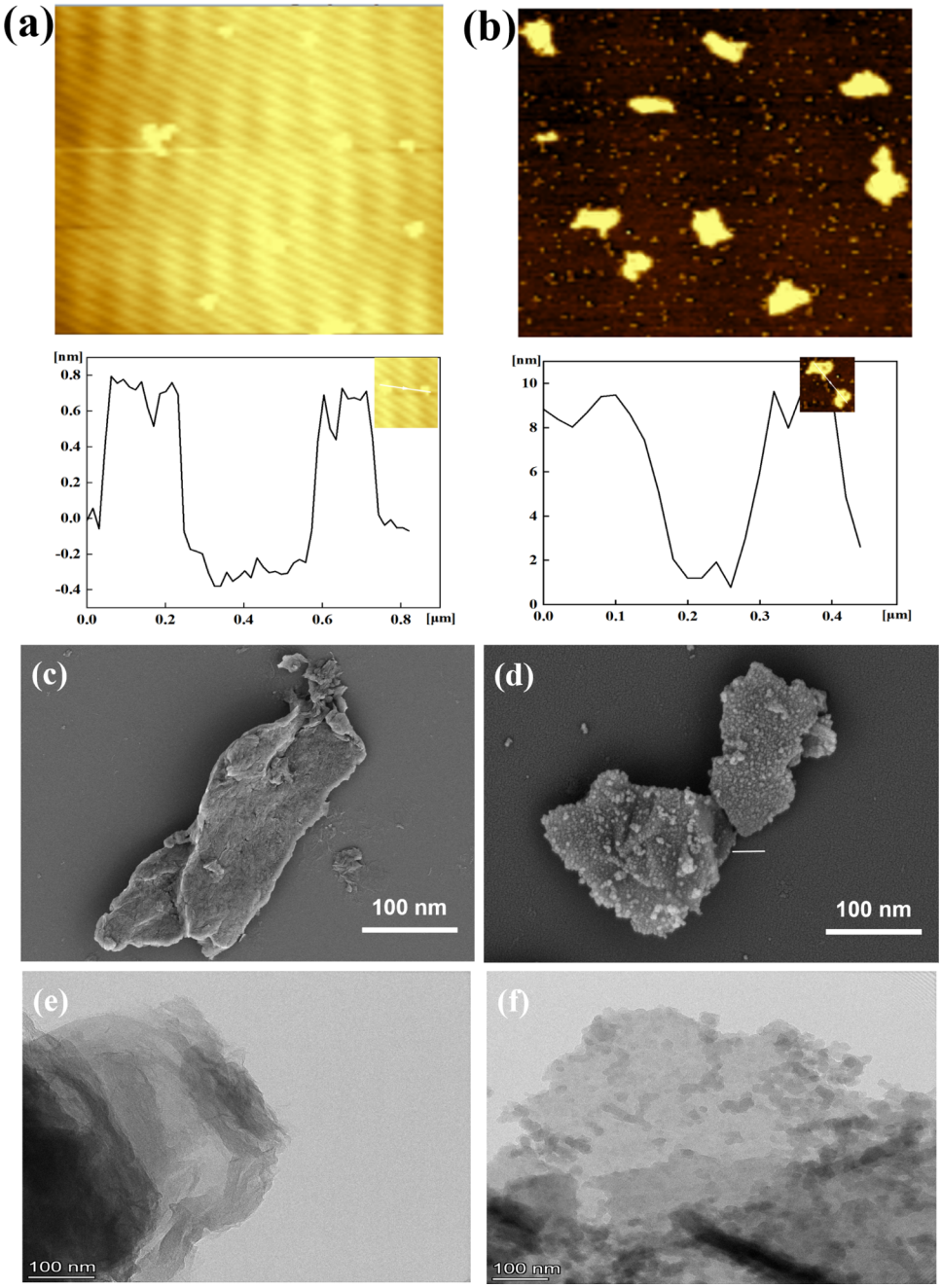

Figure 4. AFM images of (a) GO and (b) GO-SiO_2, SEM images of (c) GO and (d) GO-SiO_2, TEM images of (e) GO and (f) GO-SiO_2.

On the other hand, the thermal stability of SiO_2 is excellent, and the thermal residual weight at 800 °C is 89.4%. For GO-SiO_2, its thermal stability is significantly enhanced compared with unmodified GO. The water loss rate of GO-SiO_2 in the first stage is lower than GO, reflecting its low hydrophilicity after modification. The second weight loss temperature starts at about 200 °C, which corresponds to the decomposition of silane physically adsorbed on the surface of GO-SiO_2 and the evaporation of products produced by the self-condensation reaction of these silane molecules. The third stage starts to lose weight at 500 °C, which is mainly caused by the oxidative thermal decomposition of grafted silane and the decomposition of the carbon skeleton. Its weight loss is more gentle compared with that of GO, indicating that SiO_2 nanoparticles cover the surface of GO. Because of its strong heat resistance, it can form a barrier to prevent heat transfer and gas escape, it reduces the decomposition of the carbon skeleton of GO and enhances its thermal stability.

To further compare the morphological changes of GO before and after modification, AFM, SEM, and TEM were carried out and the results are shown in Figure 4. AFM results show that the thickness of GO layers is about 1 nm, while the thickness of GO-SiO_2 is about 10 nm, indicating that SiO_2 is introduced on the GO surface and destroys its layer spacing, and the thickness of SiO_2 coating is about 9 nm; SEM images show that the surface of GO is clean, while fine particles are evenly distributed on the surface of modified GO. TEM results show that GO has a smooth, stacked layered structure, while there are relatively uniform and obvious dark spots on the surface of GO-SiO_2, and relatively denser dark spots are

https://doi.org/10.1021/acsomega.2c04505
ACS Omega 2022, 7, 36551−36560

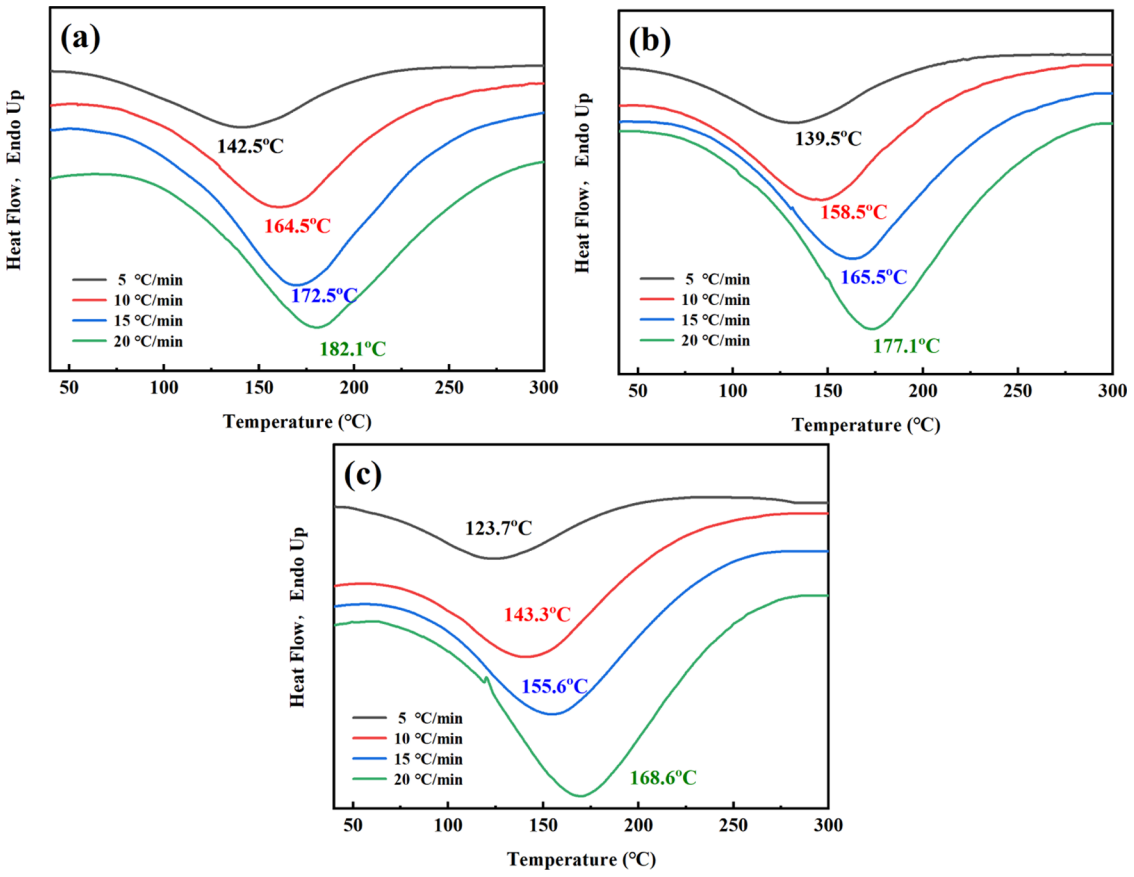

Figure 5. DSC curves of (a) pure EP, (b) EP/GO, and (c) EP/GO-SiO_2 at different heating rates.

distributed at the edge folds because the oxygen-containing functional groups at the edge of GO have higher reaction activity than those in the plane. Moreover, the stacked multilayer structure of GO-SiO_2 is reduced compared with raw GO, indicating that the incorporation of SiO_2 might reduce the thickness of the multilayer of GO. This further illustrates the successful introduction of SiO_2 on the GO surface. The dark spot diameter of GO-SiO_2 is about 10−20 nm.

3.2. Curing Kinetics Study of EP/GO Composites. EP/GO and EP/GO-SiO_2 composites were prepared, and the curing kinetics of pure EP and its nanocomposites were investigated by DSC. Figure 5 shows the curing curve of the samples at heating rates of 5, 10, 15, and 20 °C/min. The curing peak temperature (T_p) at different heating rates is calculated and plotted in Figure 5 as well.

It can be seen from Figure 5 that with the increase of temperature, the exothermic heat flow signal on the DSC curves of all three samples first showed an increasing and then a decreasing trend.

After adding unmodified GO, it can be seen that the peak temperature of curing (T_p) of EP/GO decreased slightly at about 5 °C. After adding GO-SiO_2, the T_p of EP/ GO-SiO_2 decreased by about 15−20 °C at all cooling rates, indicating that GO-SiO_2 has a more significant catalytic effect on the curing process of EP, and the reasons might be as follows:

Compared with unmodified GO, more Si−O−H and $-NH_2$ were introduced into the surface of GO-SiO_2, in which −OH can react with C−O−C of EP, thus playing an autocatalytic role, while $-NH_2$ was introduced by grafted ATPES can act as an amine curing agent and promote the curing reaction. On the other hand, SiO_2 covers the surface of GO, which can be used as the physical intermediate layer between it and the EP matrix, reducing agglomeration and better dispersion in the matrix, which is conducive to the movement between EP molecules in the later stage of the reaction.

Figure 6 shows the plots of conversion degree α versus temperature of EP, EP/GO, and EP/GO-SiO_2 at different heating rates of 5−20 °C/min, respectively. It can be seen that the conversion rate of each sample shows an S-shaped curve with temperature, indicating that all three samples have autocatalytic performance. Moreover, at all heating rates studied, it can be seen that at the same temperature, the curing degree of EP/GO-SiO_2 is the highest while that of EP is the lowest, indicating that GO-SiO_2 exhibits an enhanced promoting effect on the curing process of EP.

The curing curves of samples in Figure 5 are mathematically differentiated and the $T-d\alpha/dT$ curves of the samples were obtained, as shown in Figure 7. It can be seen from at the initial stage of curing, the curing rate of the three samples gradually increases with the progress of curing. At the later stage of curing, due to the formation of a cross-linking network, the mobility of molecules is reduced, and the curing rate gradually slows down.

Figure 7d shows that at the same temperature, the curing rate of EP/GO-SiO_2 is the highest, and the fastest reaches the maximum reaction rate, and the curing reaction is completed the first time. In contrast, the curing reaction of EP and EP/GO is relatively slow. This might be attributed to the uniform SiO_2 coating formed on the surface of GO-SiO_2, which is firmly combined and rich in −OH, $-NH_2$, and other reactive groups, which can promote the curing reaction. In addition, in

https://doi.org/10.1021/acsomega.2c04505
ACS Omega 2022, 7, 36551−36560

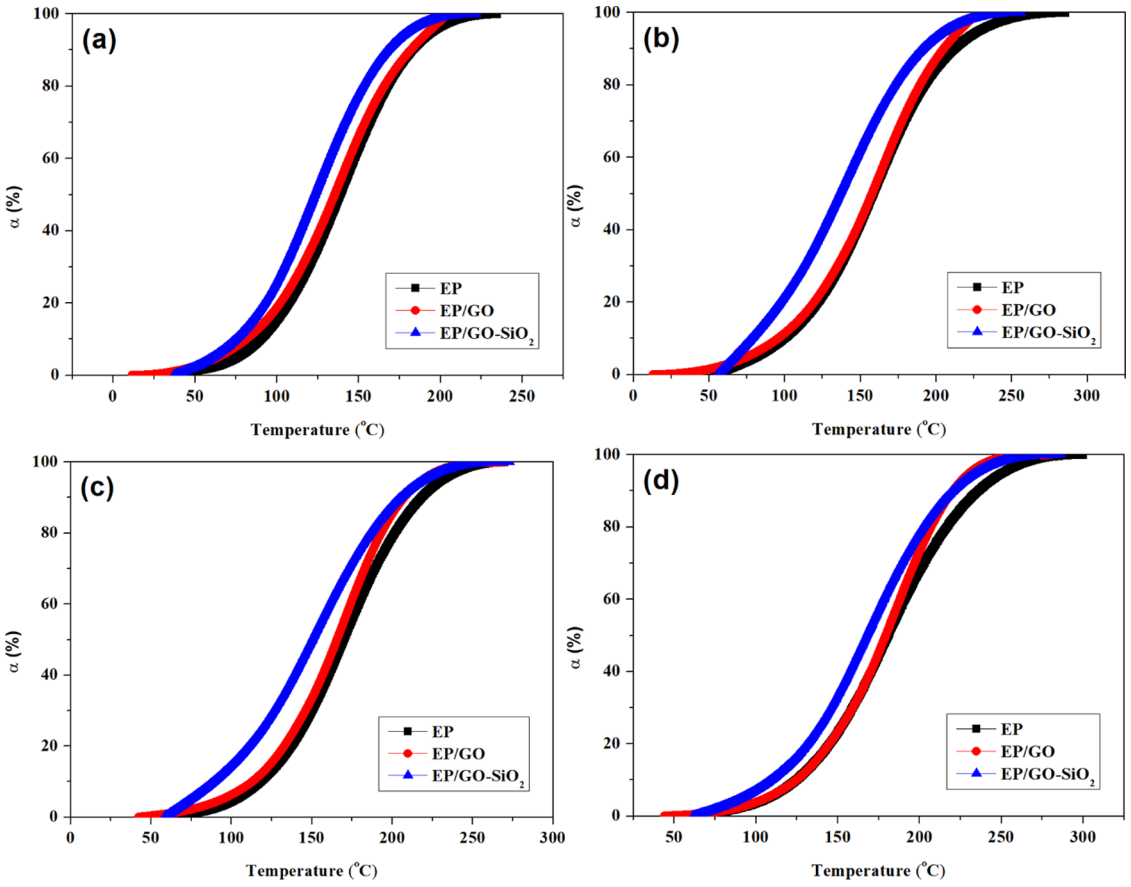

Figure 6. Conversion rate α versus temperature of EP, EP/GO, and EP/GO-SiO_2 at different heating rates: (a) 5 °C/min, (b) 10 °C/min, (c) 15 °C/min, and (d) 20 °C/min.

the late stage of the reaction, the viscosity increases significantly. The uniform coating on the surface of GO-SiO_2 can prevent the agglomeration of fillers, and improve the dispersion of GO in the matrix. Moreover, the reaction groups carried out by chemically grafted silane can form a stronger network structure with EP molecules, so as to end the curing reaction faster.

3.3. Calculation of the Curing Activation Energy. *3.3.1. Kissinger Method.* To better understand the effect of GO-SiO_2 on the curing process of EP/GO composites, the curing activation energy E_a of the samples was calculated and using the Kissinger method. The calculation formula of the Kissinger method is as follows

$$\ln\left(\frac{\beta}{T_p^2}\right) = \ln\left(\frac{A \times R}{E_a}\right) - \frac{E_a}{R} \times \frac{1}{T_p} \quad (1)$$

E_a can be determined by the slope of the $\ln(\beta/T_p^2) - 1/T_p$ plot as shown in Figure 8. The E_a of EP, EP/GO, and EP/GO-SiO_2 are 52.146, 47.935, and 38.731 kJ/mol respectively, revealing that GO-SiO_2 significantly reduces the energy barrier of curing of the composites.

3.3.2. Ozawa Method. The curing reaction process of the EP system is very complex, and during the reaction process, the curing activation energy E_a of the system changes with the change in the internal physical and chemical environment. The apparent E_a at different conversion degrees (i.e., curing degree) can be obtained by the Ozawa method, and the formula is as follows

$$\frac{\mathrm{d}[\ln(\beta)]}{\mathrm{d}(1/T_p)} = -1.052\frac{E_a}{R} \quad (2)$$

At different heating rates, when the conversion degree α is 10−90%, plots of $\ln\beta - 1/T$ of the three samples are shown in Figure 9. According to the slope of the curves in Figure 9, the apparent E_a at the same conversion can be calculated, as shown in Figure 10. It can be seen from Figure 10 that with the progress of the curing reaction, the apparent E_a of the three samples gradually increases. At the same conversion degree, E_a of pure EP is the highest, followed by EP/GO, and EP/GO-SiO_2 is the lowest. Especially in the middle and late stage of curing (with a curing degree of 50−100%), it is observed that the introduction of GO-SiO_2 significantly reduces the curing activation energy E_a of EP, indicating that the surface modification of GO can promote the whole curing process, and the promotion effect is the most obvious in the middle and late stage of curing.

Possible explanations for the above experimental phenomena are as follows: in the early stage of curing, the system is mainly controlled by chemical reactions. At this time, EP molecules and fillers are rich in reactive groups, the reaction is easy to occur, and the apparent E_a is low. Therefore, although the addition of GO or GO-SiO_2 promotes curing, the effect is not so significant at this time. With the progress of the reaction, the viscosity of the system increases, the reactive groups are gradually consumed, and the curing reaction is gradually controlled by diffusion, and the increasing viscosity also increases the difficulty of reaction molecular activity, so

https://doi.org/10.1021/acsomega.2c04505
ACS Omega 2022, 7, 36551−36560

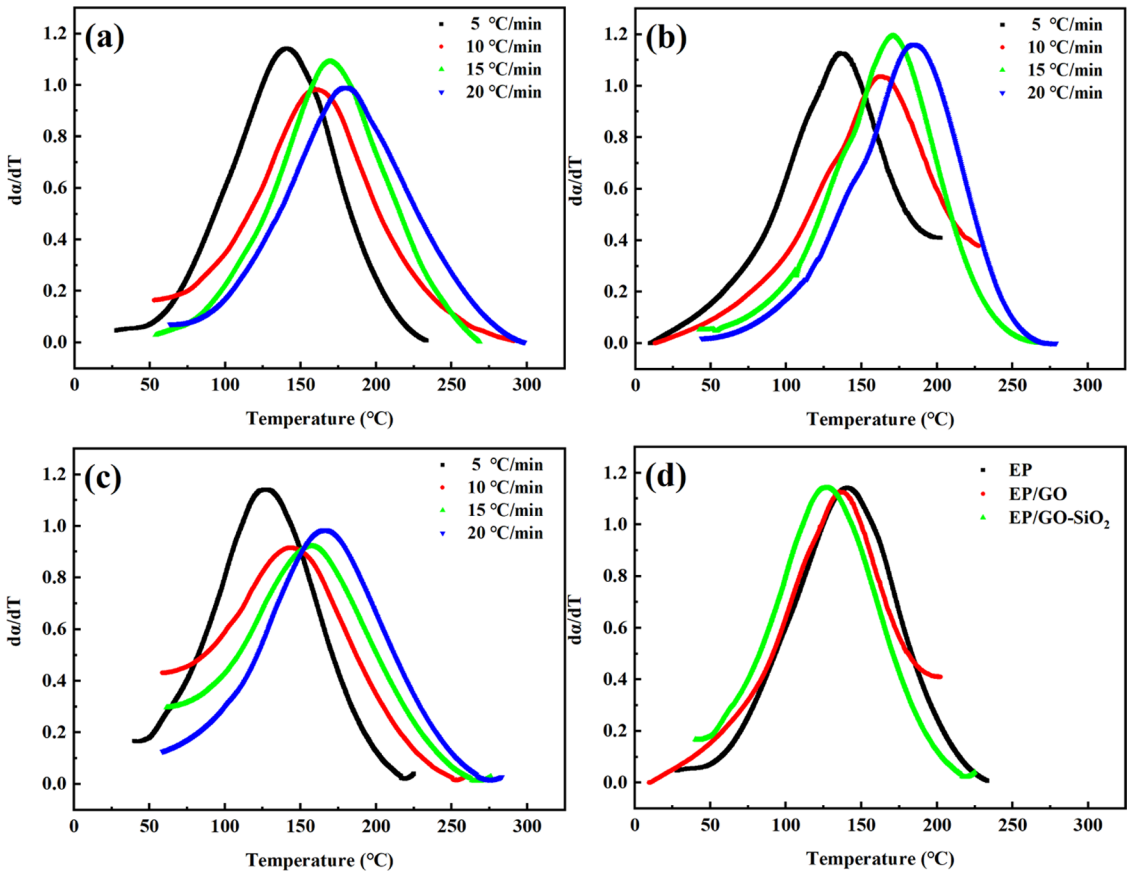

Figure 7. dα/dT versus temperature of (a) EP, (b) EP/GO, and (c) EP/GO-SiO_2 at different heating rates; (d) T−dα/dT diagram of the samples at 5 °C/min.

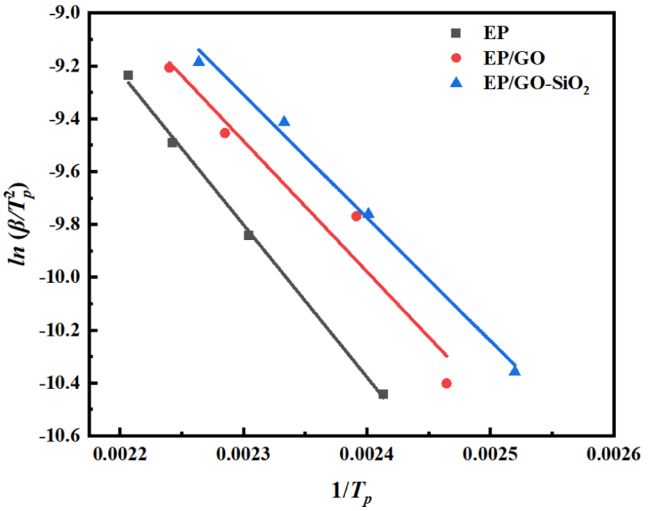

Figure 8. Kissinger plot of $\ln(\beta/T_p^2)$ versus $1000/T_p$ of EP, EP/GO, and EP/GO-SiO_2.

the apparent E_a gradually increases. At this time, there are more −OH and $-NH_2$ on the surface of GO-SiO_2, in which −OH can react with C−O−C groups to produce hydrogen bonds, which has an autocatalytic effect, and $-NH_2$ can also act as an amine curing agent to catalyze the reaction, so it plays a more significant role in promoting EP curing. In addition, the coating of GO-SiO_2 can better prevent the agglomeration of fillers, and the reactive groups of chemically grafted silane can form a stronger network structure with EP molecules, making it more compatible. Under the action of these two factors, the apparent EA of the EP/GO-SiO_2 system is lower than that of unmodified EP/GO.

4. CONCLUSIONS

Using the oxygen-containing group on the GO surface as the active site of the reaction, SiO_2 was introduced and GO-SiO_2 was successfully prepared. The chemical structure, morphology, and particle size of GO and GO-SiO_2 were compared by FT-IR, XPS, XRD, Raman, TGA, and TEM, which proved that the grafting modification was successful.

EP/GO composites were prepared by adding the above fillers (GO and GO-SiO_2) to EP. The effects of unmodified GO and GO-SiO_2 on the curing kinetics of EP were comparatively studied. The results showed that after adding unmodified GO, the peak temperature of curing (T_p) of EP/GO decreased slightly at about 5 °C; after adding GO-SiO_2, the T_p of EP/GO-SiO_2 decreased by about 15−20 °C at all cooling rates, indicating that GO-SiO_2 has a more significant catalytic effect on the curing process of EP. The calculation results of the Kissinger method showed that the curing activation energies E_a of EP, EP/GO, and EP/GO-SiO_2 were 52.146, 47.935, and 38.731 kJ/mol, respectively, revealing that GO-SiO_2 significantly reduces the energy barrier of curing of the composites. The results of the Ozawa method showed that the introduction of GO-SiO_2 reduces the curing activation energy during the whole curing process, and in the middle and late stages of curing (α = 0.5−1) can significantly reduce the curing activation energy.

https://doi.org/10.1021/acsomega.2c04505
ACS Omega 2022, 7, 36551−36560

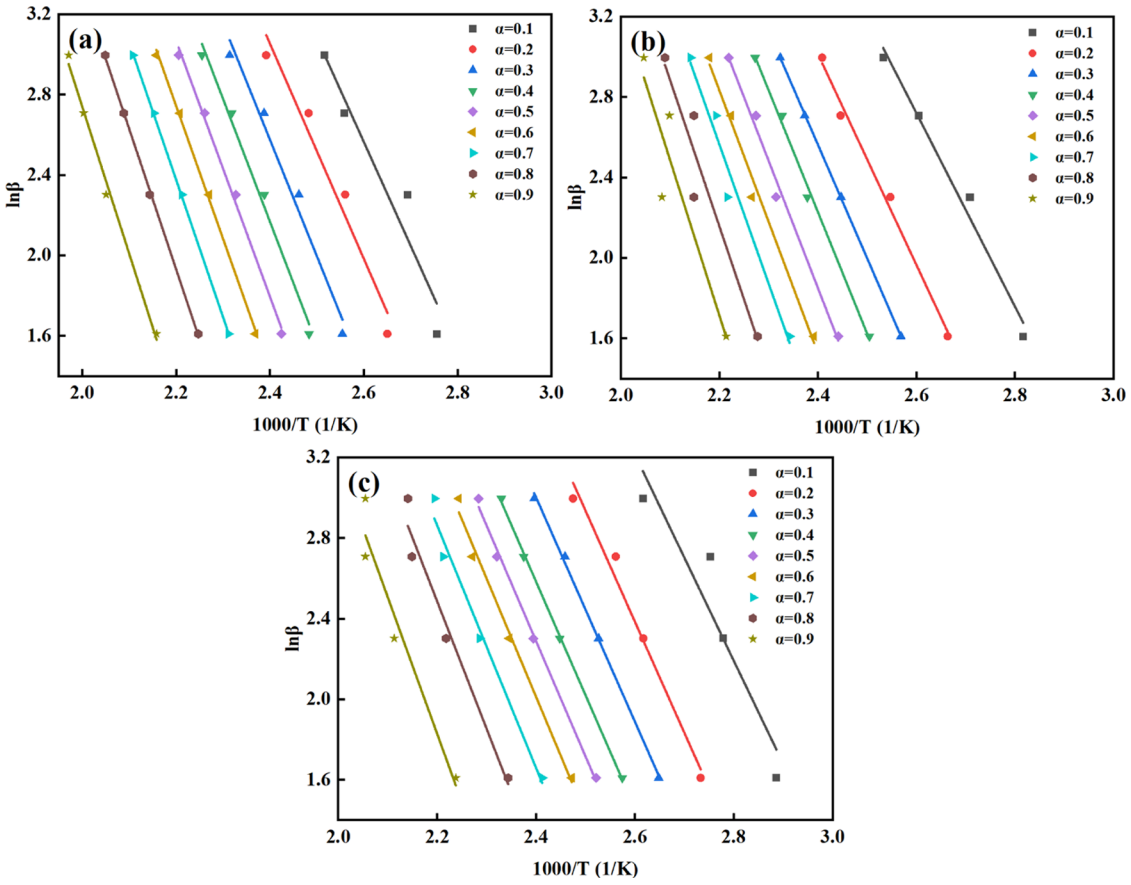

Figure 9. Fitting plots of lnβ versus 1000/T of (a) pure EP, (b) EP/GO, and (c) EP/GO-SiO_2.

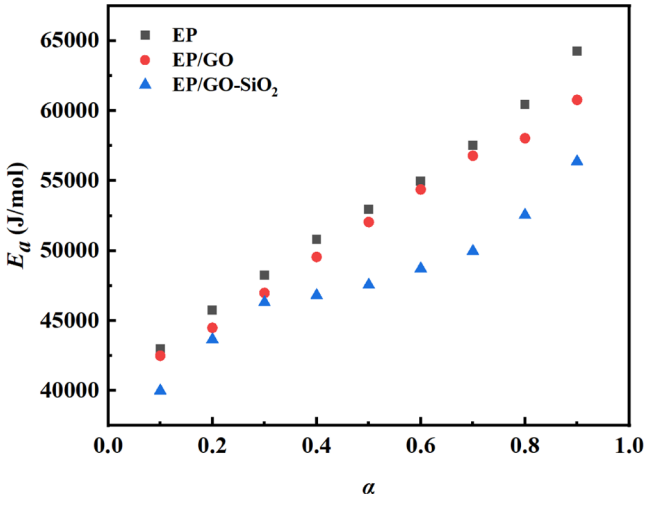

Figure 10. Changes in E_α of pure EP, EP/GO, and EP/GO-SiO_2 curing as a function of conversion α.

AUTHOR INFORMATION

Corresponding Author

Xiuduo Song − *Xi'an Modern Chemistry Research Institute, Xi'an 710065, China;* orcid.org/0000-0001-9701-6452; Email: song_xd@126.com

Authors

Bingwang Gou − *Xi'an Modern Chemistry Research Institute, Xi'an 710065, China*

Zongkai Wu − *Xi'an Modern Chemistry Research Institute, Xi'an 710065, China*

Xuebing Chen − *Xi'an Modern Chemistry Research Institute, Xi'an 710065, China*

Complete contact information is available at: https://pubs.acs.org/10.1021/acsomega.2c04505

Author Contributions

The manuscript was written through the contributions of all authors. All authors have given approval to the final version of the manuscript.

Notes

The authors declare no competing financial interest.

ACKNOWLEDGMENTS

This work was supported by the Fundamental Research Funds for the Central Universities, the National Natural Science Foundation of China (NSFC, Grant Nos. 51503134 and 51702282), and the State Key Laboratory of Polymer Materials Engineering (Grant No. SKLPME 2017-3-02).

REFERENCES

(1) Zhang, M.; Wang, H.; Nie, T.; Bai, J.; Zhao, F.; Ma, S. Enhancement of barrier and anti-corrosive performance of zinc-rich epoxy coatings using nano-silica/graphene oxide hybrid. *Corros. Rev.* **2020**, *38*, 497−513.

(2) Su, W.; Han, X.; Gong, J.; Xi, Z.; Zhang, J.; Wang, Q.; Xie, H. Toughening epoxy asphalt binder using core-shell rubber nano-particles. *Constr. Build. Mater.* **2020**, *258*, No. 119716.

(3) Damian, C. M.; Necolau, M. I.; Neblea, I.; Vasile, E.; Iovu, H. Synergistic effect of graphene oxide functionalized with SiO2 nanostructures in the epoxy nanocomposites. *Appl. Surf. Sci.* **2020**, *507*, No. 145046.
(4) Si, J.; Li, Y.; Yu, X. Curing behavior and mechanical properties of an eco-friendly cold-mixed epoxy asphalt. *Mater. Struct.* **2019**, *52*, No. 81.
(5) Javidparvar, A. A.; Naderi, R.; Ramezanzadeh, B. Epoxy-polyamide nanocomposite coating with graphene oxide as cerium nanocontainer generating effective dual active/barrier corrosion protection. *Composites, Part B* **2019**, *172*, 363−375.
(6) Apostolidis, P.; Liu, X.; Erkens, S.; Scarpas, A. Characterization of epoxy-asphalt binders by differential scanning calorimetry. *Constr. Build. Mater.* **2020**, *249*, No. 118800.
(7) Sánchez-Rodríguez, C.; Avilés, M.-D.; Pamies, R.; Carrión-Vilches, F.-J.; Sanes, J.; Bermúdez, M.-D. Extruded PLA Nanocomposites Modified by Graphene Oxide and Ionic Liquid. *Polymers* **2021**, *13*, No. 655.
(8) Yu, Y.; Zeng, F.; Chen, J.; Kang, J.; Yang, F.; Cao, Y.; Xiang, M. Effects of ordered structure on non-isothermal crystallization kinetics and subsequent melting behavior of β-nucleated isotactic polypropylene/graphene oxide composites. *J. Therm. Anal. Calorim.* **2019**, *136*, 1667−1678.
(9) Yu, W.; Sisi, L.; Haiyan, Y.; Jie, L. Progress in the functional modification of graphene/graphene oxide: a review. *RSC Adv.* **2020**, *10*, 15328−15345.
(10) Yu, Y.; Xu, R.; Chen, J.; Kang, J.; Xiang, M.; Li, Y.; Li, L.; Sheng, X. Ordered structure effects on β-nucleated isotactic polypropylene/graphene oxide composites with different thermal histories. *RSC Adv.* **2019**, *9*, 19630−19640.
(11) Ramezanzadeh, B.; Bahlakeh, G.; Mohamadzadeh Moghadam, M. H.; Miraftab, R. Impact of size-controlled p-phenylenediamine (PPDA)-functionalized graphene oxide nanosheets on the GO-PPDA/Epoxy anti-corrosion, interfacial interactions and mechanical properties enhancement: Experimental and quantum mechanics investigations. *Chem. Eng. J.* **2018**, *335*, 737−755.
(12) Ramezanzadeh, B.; Mohamadzadeh Moghadam, M. H.; Shohani, N.; Mahdavian, M. Effects of highly crystalline and conductive polyaniline/graphene oxide composites on the corrosion protection performance of a zinc-rich epoxy coating. *Chem. Eng. J.* **2017**, *320*, 363−375.
(13) Wang, M.; Ma, L.; Shi, L.; Feng, P.; Wang, X.; Zhu, Y.; Wu, G.; Song, G. Chemical grafting of nano-SiO2 onto graphene oxide via thiol-ene click chemistry and its effect on the interfacial and mechanical properties of GO/epoxy composites. *Compos. Sci. Technol.* **2019**, *182*, No. 107751.
(14) Dong, R.; Wang, L.; Zhu, J.; Liu, L.; Qian, Y. A novel SiO_2−GO/acrylic resin nanocomposite: fabrication, characterization and properties. *Appl. Phys. A* **2019**, *125*, No. 551.
(15) Zhao, X.; Li, J.; Li, Q.; Qiao, L.; Zhang, L.; Liu, Z.; Yang, C. Fabrication of a scratch & heat resistant superhydrophobic SiO_2 surface with self-cleaning and semi-transparent performance. *RSC Adv.* **2018**, *8*, 25008−25013.
(16) Bao, R.-Y.; Cao, J.; Liu, Z.-Y.; Yang, W.; Xie, B.-H.; Yang, M.-B. Towards balanced strength and toughness improvement of isotactic polypropylene nanocomposites by surface functionalized graphene oxide. *J. Mater. Chem. A* **2014**, *2*, 3190−3199.
(17) Liu, X.; Kuang, W.; Guo, B. Preparation of rubber/graphene oxide composites with in-situ interfacial design. *Polymer* **2015**, *56*, 553−562.
(18) Chen, J.; Zhang, W.; Ge, H.; Tan, J.; Liu, J. Preparation and properties of phenolic resin/graphene oxide encapsulated SiO_2 nanoparticles composites. *Polym. Eng. Sci.* **2018**, *58*, 2143−2148.
(19) Zhang, Z.; He, X.; Wang, X.; Rodrigues, A. M.; Zhang, R. Reinforcement of the mechanical properties in nitrile rubber by adding graphene oxide/silicon dioxide hybrid nanoparticles. *J. Appl. Polym. Sci.* **2018**, *135*, No. 46091.
(20) Dong, H.; Jia, Z.; Luo, Y.; Zhong, B.; Jia, D. In situ fabrication of graphene oxide supported nano silica for the preparation of rubber composites with high mechanical strength and thermal conductivity. *Polym. Compos.* **2019**, *40*, E1633−E1641.
(21) Haddadi, S. A.; Saadatabadi, A. R.; Kheradmand, A.; Amini, M.; Ramezanzadeh, M. SiO_2-covered graphene oxide nanohybrids for in situ preparation of UHMWPE/GO(SiO_2) nanocomposites with superior mechanical and tribological properties. *J. Appl. Polym. Sci.* **2019**, *136*, No. 47796.
(22) Luo, X.; Yu, K.; Qian, K. Morphologies and compression performance of graphene oxide/SiO_2 modified phenolic foam. *High Perform. Polym.* **2018**, *30*, 803−811.
(23) Bouibed, A.; Doufnoune, R. Synthesis and characterization of hybrid materials based on graphene oxide and silica nanoparticles and their effect on the corrosion protection properties of epoxy resin coatings. *J. Adhes. Sci. Technol.* **2019**, *33*, 834−860.
(24) Zhang, F.; Jiang, W.; Song, X.; Kang, J.; Cao, Y.; Xiang, M. Effects of Hyperbranched Polyester-Modified Carbon Nanotubes on the Crystallization Kinetics of Polylactic Acid. *ACS Omega* **2021**, *6*, 10362−10370.
(25) Liu, T.; Chen, D.; Cao, Y.; Yang, F.; Chen, J.; Kang, J.; Xu, R.; Xiang, M. Construction of a composite microporous polyethylene membrane with enhanced fouling resistance for water treatment. *J. Membr. Sci.* **2021**, *618*, No. 118679.
(26) Zeng, F.; Xu, R.; Ye, L.; Xiong, B.; Kang, J.; Xiang, M.; Li, L.; Sheng, X.; Hao, Z. Effects of heat setting on the morphology and performances of polypropylene separator for lithium ion batteries. *Ind. Eng. Chem. Res.* **2019**, *58*, 2217−2224.
(27) Xu, R.; Wang, J.; Chen, D.; Liu, T.; Zheng, Z.; Yang, F.; Chen, J.; Kang, J.; Cao, Y.; Xiang, M. Preparation and performance of a charge-mosaic nanofiltration membrane with novel salt concentration sensitivity for the separation of salts and dyes. *J. Membr. Sci.* **2020**, *595*, No. 117472.
(28) Zeng, F.; Chen, J.; Yang, F.; Kang, J.; Cao, Y.; Xiang, M. Effects of Polypropylene Orientation on Mechanical and Heat Seal Properties of Polymer-Aluminum-Polymer Composite Films for Pouch Lithium-Ion Batteries. *Materials* **2018**, *11*, No. 144.
(29) Xiong, B.; Chen, R.; Zeng, F.; Kang, J.; Men, Y. Thermal shrinkage and microscopic shutdown mechanism of polypropylene separator for lithium-ion battery: In-situ ultra-small angle X-ray scattering study. *J. Membr. Sci.* **2018**, *545*, 213−220.
(30) Chen, D.; Liang, Q.; Gao, F.; Liu, T.; Wu, Y.; Zheng, Z.; Kang, J.; Xu, R.; Cao, Y.; Xiang, M. Design of high-performance biomimetic reverse osmosis membranes by introducing loose liposome as an artificial water channel. *Chem. Eng. J.* **2022**, *431*, No. 133878.
(31) Wang, J.; Xu, R.; Yang, F.; Kang, J.; Cao, Y.; Xiang, M. Probing influences of support layer on the morphology of polyamide selective layer of thin film composite membrane. *J. Membr. Sci.* **2018**, *556*, 374−383.
(32) Xu, R.; Gao, F.; Wu, Y.; Ding, L.; Chen, D.; Liu, T.; Yu, Y.; Zhuo, W.; Chen, Z.; Zhang, Y.; et al. Influences of support layer hydrophilicity on morphology and performances of polyamide thin-film composite membrane. *Sep. Purif. Technol.* **2022**, *281*, No. 119884.

https://doi.org/10.1021/acsomega.2c04505
ACS Omega 2022, 7, 36551−36560